Downloaded from orbit.dtu.dk on: May 05, 2023

DTU Library

Isothermal annealing of thin rolled tungsten plates in the temperature range from 1300°C to 1400°C

Ciucani, Umberto M.; Thum, Angela; Devos, Chloé; Pantleon, Wolfgang

Published in:
Nuclear Materials and Energy

Link to article, DOI:
10.1016/j.nme.2018.03.009

Publication date:
2018

Document Version
Publisher's PDF, also known as Version of record

Link back to DTU Orbit

Citation (APA):
Ciucani, U. M., Thum, A., Devos, C., & Pantleon, W. (2018). Isothermal annealing of thin rolled tungsten plates in the temperature range from 1300°C to 1400°C. *Nuclear Materials and Energy*, *15*, 128-134. https://doi.org/10.1016/j.nme.2018.03.009

General rights
Copyright and moral rights for the publications made accessible in the public portal are retained by the authors and/or other copyright owners and it is a condition of accessing publications that users recognise and abide by the legal requirements associated with these rights.

- Users may download and print one copy of any publication from the public portal for the purpose of private study or research.
- You may not further distribute the material or use it for any profit-making activity or commercial gain
- You may freely distribute the URL identifying the publication in the public portal

If you believe that this document breaches copyright please contact us providing details, and we will remove access to the work immediately and investigate your claim.

Nuclear Materials and Energy 15 (2018) 128–134

Contents lists available at ScienceDirect

Nuclear Materials and Energy

journal homepage: www.elsevier.com/locate/nme

Isothermal annealing of thin rolled tungsten plates in the temperature range from 1300 °C to 1400 °C

Umberto M. Ciucani*, Angela Thum, Chloé Devos, Wolfgang Pantleon

Section of Materials and Surface Engineering, Department of Mechanical Engineering, Technical University of Denmark, 2800 Kongens Lyngby, Denmark

ARTICLE INFO

Keywords:
Tungsten
Annealing
Recrystallization
Thermal stability
Hardness testing
EBSD

ABSTRACT

The annealing behavior of thin tungsten plates of four different thicknesses achieved by warm- and (in two cases) cold-rolling is investigated. Isothermal experiments at five different temperatures between 1300 °C to 1400 °C were performed. Hardness testing of annealed specimens allowed tracking the degradation of the mechanical properties and, indirectly, the microstructural evolution. Supplementary microscopical investigations of the microstructure in the as-received state as well as after annealing were performed to characterize the initial condition and to support the identification of the involved restoration processes. All four tungsten plates undergo microstructural restoration by recovery and recrystallization. The observed differences in their behavior were rationalized in terms of the identified differences in the microstructure in the as-received state, rather than their different initial thickness.

1. Introduction

One of the most critical components of future fusion reactors are the plasma-facing components of the blanket and the divertor. They will be exposed to high particle and high heat fluxes, requiring superior performance in terms of thermal stability and mechanical resistance. Tungsten meets many of the requirements for plasma-facing components [1]: a high thermal conductivity (164 W/mK), high strength, high yield point and creep resistance at high temperatures, highest melting point of all metals (3422 °C), and a low sputtering yield due to a high sputtering threshold energy [2,3]. In an annealed state, tungsten shows an intrinsic brittleness at room temperature [4–7] and a rather high ductile-to-brittle transition temperature [8–10]. After plastic deformation, tungsten behaves ductile even at room temperature. Operation of plastically deformed tungsten parts at higher temperatures is nevertheless limited by the occurrence of recrystallization replacing the ductile, deformed microstructure by an intrinsically brittle one. Following earlier studies on rolled foils [11–13] and plates [14–16], the annealing behavior of thin tungsten plates is characterized with focus on recrystallization; the main interest being whether a reduced thickness can lead to an improved performance in view of the thermal activated processes occurring during annealing.

2. Materials and methods

Four plates with four different thicknesses (2 mm, 1 mm, 0.5 mm and 0.2 mm) of 99.97% technically pure tungsten [17], produced via conventional powder metallurgical route were acquired from Plansee SE (Reutte, Austria). The interstitial impurity content of the plates is below 5 ppm for Hydrogen and Nitrogen, below 20 ppm for Oxygen and below 30 ppm for Carbon, as guaranteed by the manufacturer. The thin plates (TP) with sizes 100 mm × 250 mm × *thickness* were cut from larger pieces not specified in any more detail by the manufacturer. According to the specifications of the manufacturer, the two plates with larger thicknesses (2 mm (TP2) and 1 mm (TP1)) were obtained by warm-rolling, whereas the two plates with smaller thicknesses (0.5 mm (TP0.5) and 0.2 mm (TP0.2)) were achieved by final cold-rolling steps. From the thin plates, rectangular samples of 3 mm × 4 mm × plate *thickness* were cut for annealing, with their long side corresponding to the long direction of the as-received plates, so that the different directions can be identified later. To prevent high temperature oxidation during annealing, the specimens were encapsulated in glass ampoules. Each ampoule contained four different specimens, one from each of the TPs, in an argon atmosphere.

Isothermal annealing of the small specimens was performed in a general-purpose tube furnace NaberTherm RHTC 80-230/15 between 1300 °C and 1400 °C at five specific temperatures for times up to 67 h. Although rolling reduces porosity and homogenises the microstructure within the plates compared to the as-sintered condition, heterogeneities within the rolled plates are expected. Therefore, a large number of isothermal annealings for different time periods are performed for each annealing temperature to ensure the validity of the results.

* Corresponding author.
E-mail address: umciuc@mek.dtu.dk (U.M. Ciucani).

https://doi.org/10.1016/j.nme.2018.03.009
Received 14 December 2017; Received in revised form 2 March 2018; Accepted 17 March 2018
Available online 28 March 2018
2352-1791/ © 2018 Elsevier Ltd. This is an open access article under the CC BY-NC-ND license (http://creativecommons.org/licenses/BY-NC-ND/4.0/).

The microstructure of the material was assessed by Light Optical Microscopy (LOM), Electron Back-Scatter Diffraction (EBSD) and Vickers hardness testing. For light optical microscopy, conventional metallographic preparation by mechanical grinding and polishing was performed. In a final step, the specimens were etched with Murakami's etchant (10 g NaOH, 10 g $K_3Fe(CN)_6$ in 100 ml distilled water). Rolling direction (RD) and transverse direction (TD) of each plate were identified through LOM on different sections: while three of the rectangular plates were cut by the manufacturer with their long direction along RD, TP2 was cut with the long side along TD. This difference between the cuts was taken into account when investigating the microstructure in specific individual sections.

After conventional metallographic preparation, cross sections containing RD and the normal direction (ND) were prepared for EBSD by electropolishing using an aqueous solution containing 3 wt% NaOH at RT with an applied voltage of 12 V and a current of approximately 2 A for times ranging from 15 s to 75 s for the thinnest and the thickest plates, respectively. EBSD investigations were performed with a Bruker NOVA NanoSEM with an applied voltage of 20 kV and a step size of 100 nm. For each plate orientation maps of 100.8 µm × 86.9 µm (100.8 µm × 86.5 µm in case of TP0.2) were acquired.

Hardness testing was performed with a Vickers indenter and a load of 0.5 kg on the outer surface of the plates parallel to the rolling plane, i.e. containing RD and TD, in the as-received as well as the annealed condition to track the changes of the mechanical properties during annealing. For each condition, at least 10 indents were analyzed, the smallest and the largest of which were discarded and the average hardness values obtained from the remaining are reported together with the standard deviation of the average.

3. Results

3.1. Thin plates in as-received

The hardness values of the as-received plates are summarized in Table 1. In general, the thin plates showed an increased hardness with reduced thickness, from 550 ± 3 HV0.5 for TP2 to 642 ± 2 HV0.5 for TP0.2, as expected from an increased thickness reduction by rolling. The plate TP1, however, did not follow this trend and showed an exceptionally low hardness of 541 ± 2 HV0.5 which must have been caused by a difference in manufacturing of the plate (cf. Section 4).

Large orientation maps were obtained by EBSD on the longitudinal section (containing RD and ND) and shown in Fig. 1. The maps reveal the typical microstructural features after thickness reduction by rolling. The grains are elongated along the rolling direction with an aspect ratio increasing, in general, with decreasing plate thickness. Where the aspect ratio of the grains in the two thicker plates, TP2 and TP1, appear quite similar, a much higher aspect ratio is observed in TP0.5 and TP0.2 due to the (additional) cold-rolling. As a measure of the grain size, the average chord length between high angle boundaries (with disorientation angles above 15°) was determined along ND by the line intercept method. As obvious from Table 2, a smaller average chord length is observed in general for the plates with smaller thicknesses. The cold-rolled plates TP0.5 and TP0.2 show a much smaller chord length compared to the values of the thicker plates TP2 and TP1 which have been warm-rolled only. The slightly larger chord length of TP1 (564 ± 12 nm) compared to TP2 (538 ± 17 nm) supports the suspicion that TP1 has a different manufacturing history.

From the orientation data collected by EBSD, the 100 pole figure is derived for each TP and shown in Fig. 1(e)–(h). The pole figures reveal the existence of a single, preferential texture component, the rotated cube component {100}⟨011⟩, for all four plates. As summarized in Table 2, the strength of the texture as quantified by either the maximum 100 pole density or the volume fraction of the {100}⟨011⟩ component (allowing a deviation of 15° from the ideal orientation) increases with decreasing plate thickness from 35% to 57%, with exception of TP1 showing not only a much weaker texture (with maximum pole density of 4.2), but also a much lower volume fraction (13%) of the {100}⟨011⟩ component than all other plates.

Table 1
Vickers hardness values (HV0.5) for four thin tungsten plates in the as-received, severely recovered and fully recrystallized condition after isothermal annealing at 1325 °C. The hardness values obtained with 0.5 kgf are reported as average values with the standard deviation of the average value.

	HV_{def}	HV_{rec}	HV_{rex}	HV_{def} - HV_{rec}
TP2	550 ± 3	492 ± 2	449 ± 2	58
TP1	541 ± 2	507 ± 2	449 ± 1	38
TP0.5	595 ± 3	475 ± 2	414 ± 1	120
TP0.2	642 ± 2	479 ± 2	415 ± 3	163

3.2. Thin plates after isothermal annealing

Isothermal annealing was performed at five temperatures (1300 °C, 1325 °C, 1350 °C, 1375 °C, and 1400 °C) for times up to 67 h. The hardness values determined on the rolling planes are summarized in Fig. 2 for all four thin plates.

In general, the hardness decreases with the progress of annealing in a characteristic manner involving two different stages. These are indicated in Fig. 3 on the example of the behavior of all four plates during annealing at 1325 °C. Both stages are characterized by an initial hardness drop followed by a stagnation period leading to an apparently constant hardness value. The first, rapid initial drop in hardness from the as-received state is related to recovery processes in the deformed microstructure reducing its stored energy. Caused by this reduction in the driving force for recovery, the progress of recovery slows down leading to an apparent stagnation period, corresponding to a very late phase of recovery. The second hardness reduction occurring in a slightly milder manner is caused by recrystallization and leads to a second stagnation stage of constant hardness, attributed to complete recrystallization. Table 1 compares the hardness values of both stagnation stages obtained after annealing at 1325 °C, i.e. in the late phase of recovery and after complete recrystallization. The hardness values for the first apparent stagnation stage (attributed to severe recovery) are slightly lower for the two cold-rolled, thinner plates than for the two warm-rolled, thicker plates. In general, the average hardness loss due to recovery ($HV_{def} - HV_{rec}$) increases with decreasing plate thickness, except for TP1 which shows the smallest hardness loss due to recovery of all plates (see Table 1). Similar trends are observed for the hardness values of the second stagnation stage corresponding to complete recrystallization.

Comparing the hardness evolution at all different temperatures in Fig. 2, the stagnation values for the hardness after severe recovery seem not to be largely different, while rather different hardness values for the fully recrystallized states are observed for the different annealing temperatures. Peculiar behaviors at both, the lowest and highest annealing temperature are observed: for isothermal annealing at 1300 °C, only a single restoration stage is clearly identified; after 2 h the hardness has already dropped to a low value due to recovery and stays rather unaltered up to the largest annealing time of 67 h indicating contuation of recovery. For all four thin plates,the occurrence of recrystallization may still be questioned. On the other, for isothermal annealing at 1400 °C, a further decrease in hardness is observed after 16 h. This third stage of hardness reduction is attributed to grain growth occurring after completion of recrystallization.

Such an assignment of the dominant microstructural processes to the different annealing stages in the hardness evolution is confirmed by metallographical observations. Fig. 4 presents light optical micrographs from TP2 after different periods of annealing at 1325 °C. Fig. 4(a) shows the elongated grain structure after warm-rolling and resembles closely the orientation map of the same condition in Fig. 1(a). With increasing

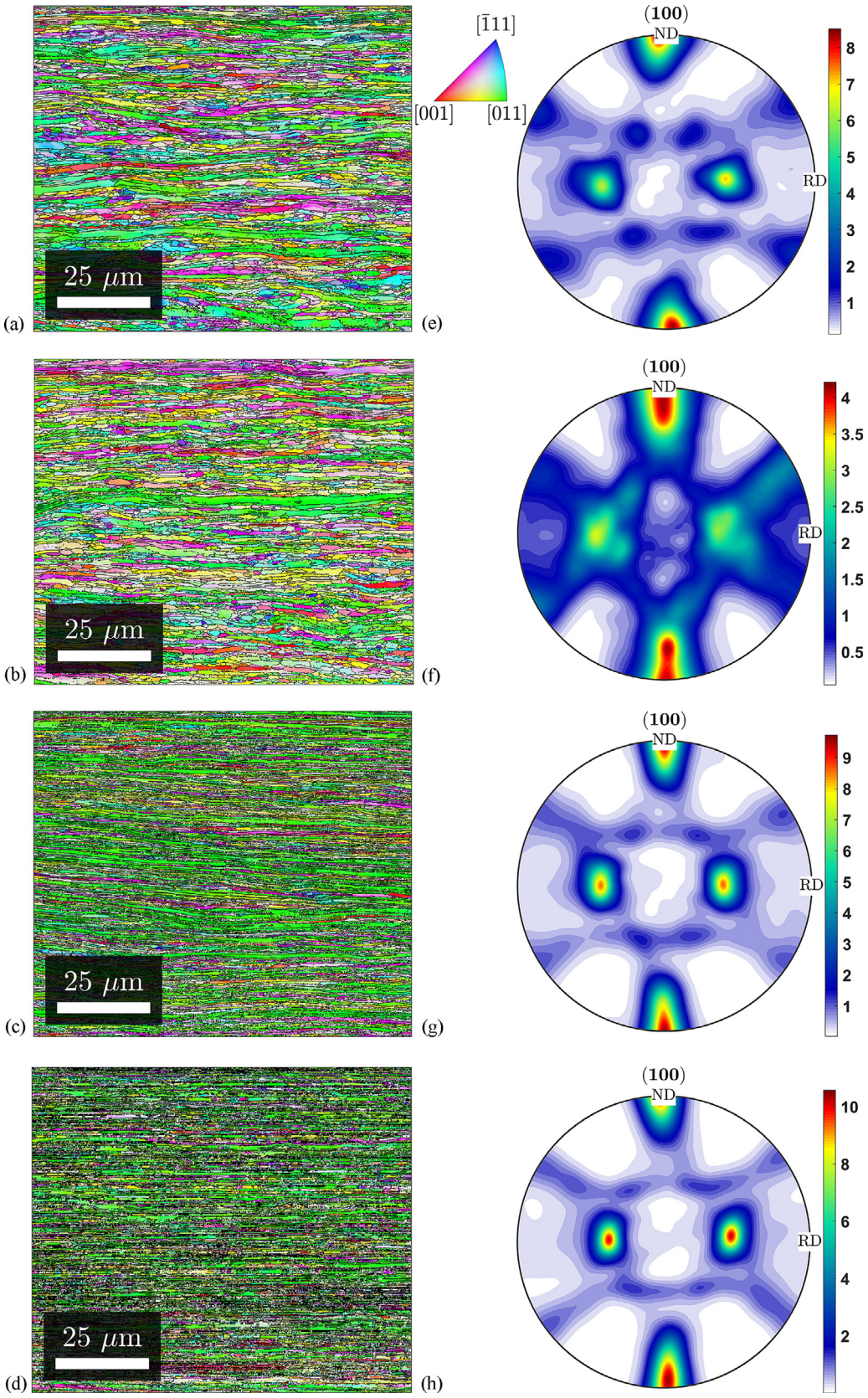

Fig. 1. Orientation maps of the as-received condition obtained by EBSD on the RD/ND section (with RD being horizontally) in the center of the specimen (a) TP2, (b) TP1, (c) TP0.5 and (d) TP0.2. The colors represent the crystallographic direction along RD according to the inverse pole figure in the insert. (e), (f), (g) and (h) show the corresponding 100 pole figures with the pole density given in terms of multiple random.

Table 2
Quantitative characterisation of the microstructure in the as-received thin plates as obtained by EBSD. The volume fraction of the rotated cube component is determined allowing a maximal deviation of 15° from the ideal orientation.

	Average chord length along ND (nm)	Maximal (100) pole density (times multiple random)	Volume fraction of rotated cube {100}⟨011⟩ component
TP2	538 ± 17	8.5	35%
TP1	564 ± 12	4.2	13%
TP0.5	327 ± 3	9.7	48%
TP0.2	229 ± 4	11.0	57%

annealing time, the elongated grain structure is progressively replaced by an equiaxed grain structure due to recrystallization. Fig. 4(b) and (c) represent partially recrystallized conditions after 4 h and 16 h, respectively, whereas Fig. 4(d) represents the fully recrystallized state achieved after 24 h.

Additionally, a microstructural heterogeneity throughout the plate is revealed by LOM in Fig. 4. The lower part of the images, corresponding to the region close to the open surface which during rolling has been in contact with the rolls, shows a different stage of the microstructural evolution where recrystallization has been retarded. For instance, the outer layer in Fig. 4(b) resembles more the as-received condition and elongated grains can still be traced after 4 h of annealing. This explains why the observed hardness values after 4 h of annealing at 1325 °C as measured by indenting the rolling surface, did not show evidence for recrystallization, but rather indicate a late stage of recovery (cf. Fig. 3). The central part of the plate recrystallizes earlier than the outer parts. From Fig. 4(d), on the other hand, complete recrystallization of the entire plate can be concluded. This is confirmed by Fig. 5(a) revealing the microstructure of TP2 after annealing at 1325 °C for 24 h with larger magnification.

Comparing the fully recrystallized microstructure with a hardness of 449 ± 2 HV0.5 in Fig. 5(a) with the microstructure of TP2 after annealing at 1400 °C for 48 h having a hardness of 428 ± 1 HV0.5 shown in Fig. 5(b), a larger grain size can be recognized in the latter. The difference of about 30 HV0.5 is attributed to grain growth lastly occurring in the outer layer after complete recrystallization.

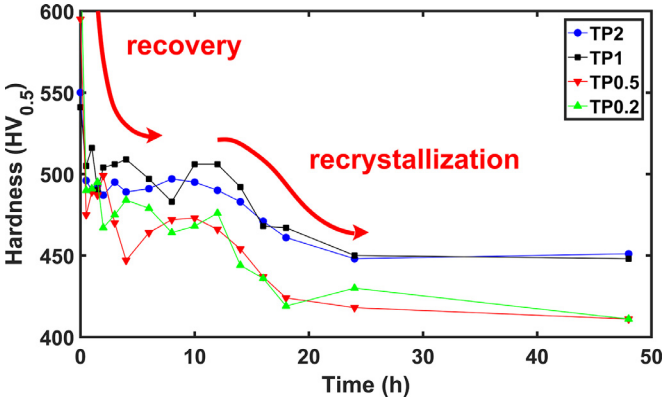

Fig. 3. Hardness evolution of all four thin plates during isothermal annealing at 1325 °C indicating the different stages of recovery and recrystallization. (The standard deviations of the average values are in all cases smaller than the markers.).

The microstructural heterogeneity imposed by the rolling conditions and inherited to the annealed microstructures was assessed for TP2 by hardness profiles along ND. The microhardness profiles shown in Fig. 6 were obtained by indenting with a Vickers indenter and a small load of 50 gf on the RD/ND section at different distances from the open surface which have been in contact with the rolls. Care was taken to displace the different indents more than 2.5 times their diagonal from each other. The obtained profiles after annealing (Fig. 6(a) and (b)) reveal an exponential decrease in hardness with increasing distance from the outer rolling surface:

$$HV(x) = HV_{center} + (HV_{surface} - HV_{center})\exp(-x/\lambda).$$

The hardness is significantly higher (up to 60 HV0.05) in a surface layer of about 150 nm than in the recrystallized center of the plate (cf. Table 3). With increasing annealing time, the size of the outer layer is reduced due to the progress of recrystallization there.

As seen from the microhardness profile through the entire plate TP2

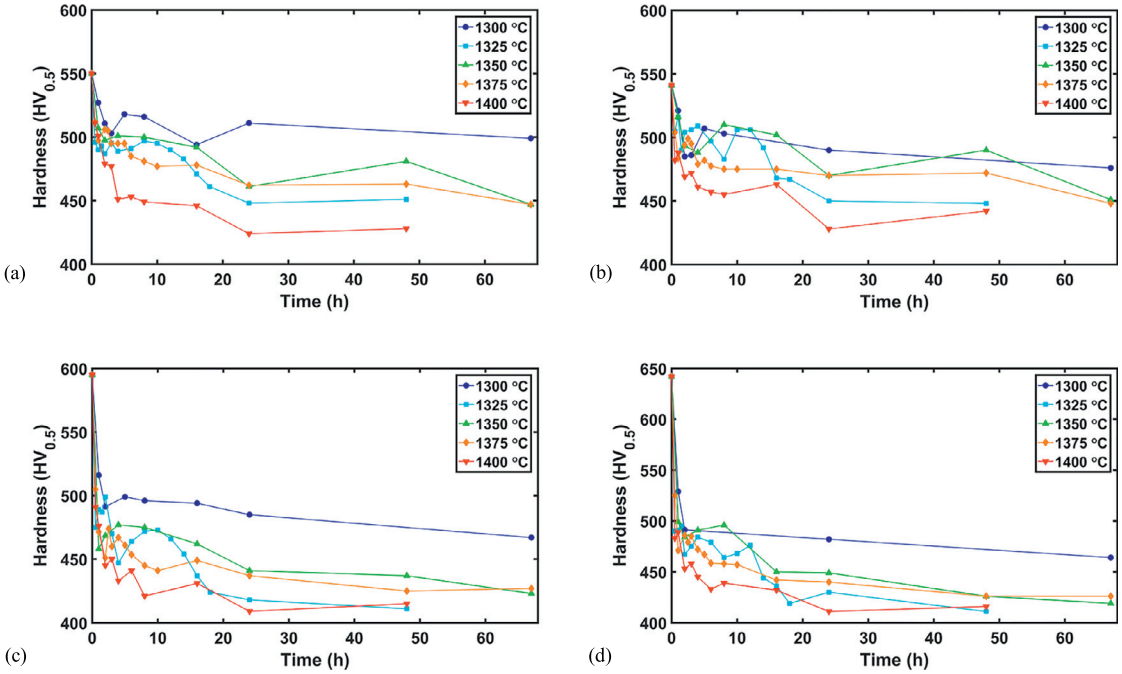

Fig. 2. Hardness evolution of the thin plates after isothermal annealing up to 67 h at five different temperatures between 1300 °C and 1400 °C as obtained on the rolling plane. (a) TP2, (b) TP1, (c) TP0.5 and (d) TP0.2. (The standard deviations of the average values are in all cases smaller than the markers.).

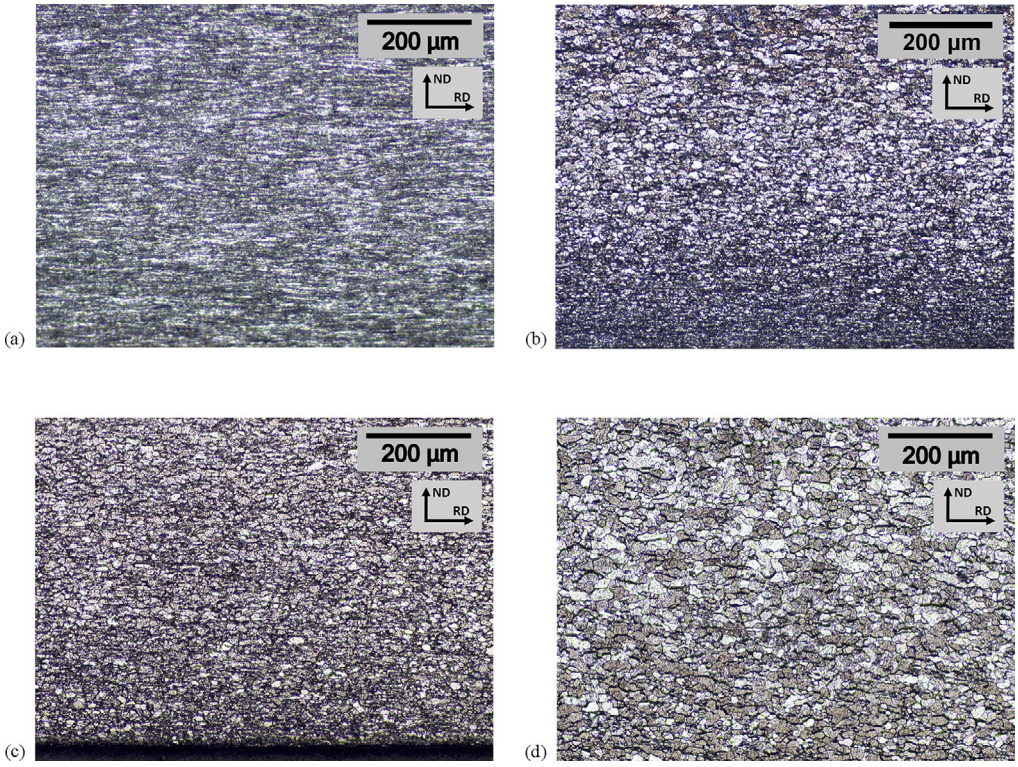

Fig. 4. Light optical micrographs of warm-rolled TP2 in the as-received condition (a) and after isothermal annealing at 1325 °C for (b) 4 h, (c) 16 h and (d) 24 h. Rolling and normal direction are indicated; the lower part of the images is close to the outer rolling surface of the plate.

in the as-received condition shown in Fig. 6(c), the initial variation in hardness across the plate is less pronounced (40 HV0.05) with a slightly asymmetrical distribution. Despite the higher hardness in the outer layers of the plate in the as-received condition and hence a higher stored energy there, recrystallization of the outer layers occurs last.

4. Discussion

The hardness of the thin plates in their as-received condition should reflect the plastic work put into the material during rolling with a larger thickness reduction (and hence,presuming the same initial height, a smaller thickness) corresponding to a higher hardness value. This expectation is satisfied in general, disrupted though by the too low hardness of TP1 only. The deviating behavior of TP1 is further substantiated by inspecting the microstructure of the as-received state using EBSD. For TP1, the average chord length along ND, is slightly larger than that of TP2 (instead of smaller as expected from presumed further rolling). The strength of the deformation texture and the volume fraction of the characteristic rotated cube texture component {100} ⟨011⟩ are both lower than for all other plates. Finally, the hardness loss during recovery is smaller for TP1 than for all the other plates indicating that the driving force for recovery has been lower for this plate as confirmed by the lower initial hardness. All findings can be rationalized by presuming that TP1 may have been manufactured in a deviating manner than the other plates. Unfortunately, details of the processing of the plates were not revealed by the manufacturer and the received cuts might originate from different batches. Even if the same rolling sequence was applied on material from the same batch, TP1 may have recrystallized either dynamically during one of the passes of warm-rolling or statically during an intermediate annealing between some of the warm-rolling passes. Nevertheless, TP1 in its as-received state shows a typical deformed microstructure after warm-rolling without any indication for partial recrystallization; no evidence for any recrystallized volume fraction is gained from the orientation data in

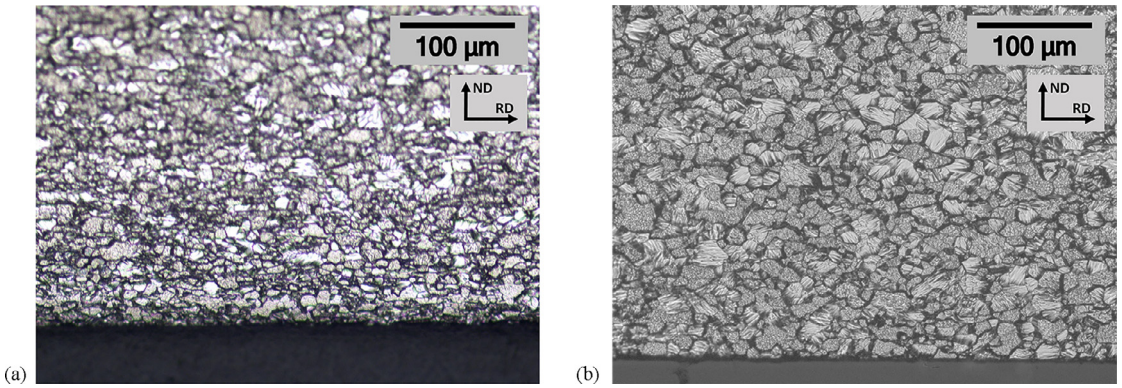

Fig. 5. Light optical micrographs of warm-rolled TP2 after isothermal annealing (a) at 1325 °C for 24 h and (b) at 1400 °C for 48 h. Rolling and normal direction are indicated; the lower part of the images is close to the outer rolling surface of the plate.

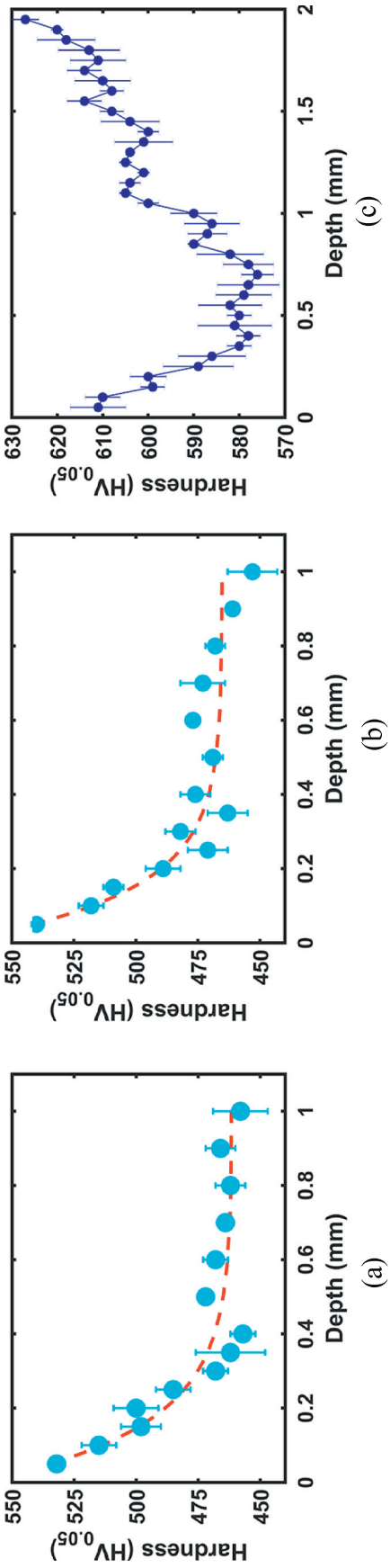

Fig. 6. Microhardness profiles along ND obtained by Vickers indentation with 50 gf on an RD/ND section for TP2 after annealing at 1325 °C for (a) 4 h and (b) 8 h and (c) in the as-received condition.

Table 3
Fitting parameters for the exponential decrease describing the hardness profile along ND in TP2 after annealing at 1325 °C .

Annealing time (h)	HV_{center}	$HV_{surface}$	Decay length λ (nm)
4	461	563	150
8	465	576	132

Fig. 1(b) ruling out that recrystallization has happened during the last rolling pass. Consequently, the thickness of the plates is not decisive for their annealing behavior. Yet, if the plates are ordered with respect to their initial hardness (as indicator of the stored energy in the deformation structure) instead of the plate thickness, all observations follow a common trend between the four plates revealing a systematic dependence on the initial hardness.

5. Conclusions

The annealing behavior of four rolled plates of pure tungsten with different thicknesses has been characterized in terms of their combined microstructural and hardness evolution. Different stages in the hardness evolution have been attributed to different microstructural restoration processes and confirmed by microstructural investigations. A systematic dependence of the annealing behavior on the initial hardness, but not on the initial plate thickness has been identified and discussed. The comprehensive data set for isothermal annealing at five different temperatures can form an indispensible basis for a quantitive analysis of the restoration kinetics of these thin tungsten plates, in particular for quantification of the recrystallization kinetics.

Acknowledgments

This work has been carried out partially within the framework of the EUROfusion Consortium. The views and opinions expressed herein do not necessarily reflect those of the European Commission.

References

[1] J. Davis, V. Barabash, A. Makhankov, L. Plöchl, K. Slattery, Assessment of tungsten for use in the ITER plasma facing components, J. Nucl. Mater 258–263 (1998) 308–312, http://dx.doi.org/10.1016/S0022-3115(98)00285-2.
[2] E. Lassner, W.-D. Schubert, The *element tu*ngsten, Tungsten, (1999), pp. 1–59, http://dx.doi.org/10.1007/978-1-4615-4907-9_1.
[3] R.G. Abernethy, Predicting the performance of tungsten in a fusion environment: a literature review, Mater. Sci. Technol. 836 (2016) 1–12, http://dx.doi.org/10.1080/02670836.2016.1185260.
[4] B. Gludovatz, S. Wurster, A. Hoffmann, R. Pippan, Fracture toughness of polycrystalline tungsten alloys, Int. J. Refract. Met. Hard Mater 28 (2010) 674–678, http://dx.doi.org/10.1016/j.ijrmhm.2010.04.007.
[5] D. Rupp, R. Mönig, P. Gruber, S.M. Weygand, Fracture toughness and microstructural characterization of polycrystalline rolled tungsten, Int. J. Refract. Met. Hard Mater. 28 (2010) 669–673, http://dx.doi.org/10.1016/j.ijrmhm.2010.05.006.
[6] D. Rupp, S.M. Weygand, Experimental investigation of the fracture toughness of polycrystalline tungsten in the brittle and semi-brittle regime, J. Nucl. Mater 386–388 (2009) 591–593, http://dx.doi.org/10.1016/j.jnucmat.2008.12.184.
[7] B. Gludovatz, S. Wurster, T. Weingärtner, a. Hoffmann, R. Pippan, Influence of impurities on the fracture behaviour of tungsten, Philos. Mag. 91 (2011) 3006–3020, http://dx.doi.org/10.1080/14786435.2011.558861.
[8] M. Rieth, B. Dafferner, Limitations of W and W-1%La2O3 for use as structural materials, J. Nucl. Mater 342 (2005) 20–25, http://dx.doi.org/10.1016/j.jnucmat.2005.03.013.
[9] M. Rieth, A. Hoffmann, Influence of microstructure and notch fabrication on impact bending properties of tungsten materials, Int. J. Refract. Met. Hard Mater. 28 (2010) 679–686, http://dx.doi.org/10.1016/j.ijrmhm.2010.04.010.
[10] M. Rieth, A. Hoffmann, Impact bending tests on selected refractory materials, Adv. Mater. Res. 59 (2009) 101–104, http://dx.doi.org/10.4028/www.scientific.net/AMR.59.101.
[11] J. Reiser, M. Rieth, B. Dafferner, Tungsten foil laminate for structural divertor applications – basics and outlook, J. Nucl. Mater 423 (2012) 1–8, http://dx.doi.org/10.1016/j.jnucmat.2012.01.010.
[12] J. Reiser, M. Rieth, B. Dafferner, A. Hoffmann, X. Yi, D.E.J. Armstrong, Tungsten foil laminate for structural divertor applications - Analyses and characterisation of

tungsten foil, J. Nucl. Mater. 424 (2012) 197–203, http://dx.doi.org/10.1016/j.jnucmat.2013.01.295.
[13] T. Palacios, J. Reiser, J. Hoffmann, M. Rieth, A. Hoffmann, J.Y. Pastor, Microstructural and mechanical characterization of annealed tungsten (W) and potassium-doped tungsten foils, Int. J. Refract. Met. Hard Mater. 48 (2015) 145–149, http://dx.doi.org/10.1016/j.ijrmhm.2014.09.005.
[14] A. Alfonso, D. Juul Jensen, G.N. Luo, W. Pantleon, Recrystallization kinetics of warm-rolled tungsten in the temperature range 1150–1350 °C, J. Nucl. Mater. 455 (2014) 591–594, http://dx.doi.org/10.1016/j.jnucmat.2014.08.037.
[15] A. Alfonso, D. Juul Jensen, G.N. Luo, W. Pantleon, Thermal stability of a highly-deformed warm-rolled tungsten plate in the temperature range 1100–1250 °C, Fusion Eng. Des. 98–99 (2015) 1924–1928, http://dx.doi.org/10.1016/j.fusengdes.2015.05.043.
[16] S. Bonk, J. Reiser, J. Hoffmann, A. Hoffmann, Cold rolled tungsten (W) plates and foils: evolution of the microstructure, Int. J. Refract. Met. Hard Mater. 60 (2016) 92–98, http://dx.doi.org/10.1016/j.ijrmhm.2016.06.020.
[17] PLANSEE SE, Pure-W Specifications, (2017). https://www.plansee.com/en/materials/tungsten.html.